Korean J. Chem. Eng., **29**(10), 1444-1452 (2012)
DOI: 10.1007/s11814-012-0009-0

Preparation of spherical macroporous silica in an aerosol phase

Ki Woong Ahn, Hana Rah, and Sun-Geon Kim†

School of Chemical Engineering and Materials Science, Chung Ang University,
221, Huksuk-dong, Dongjak-gu, Seoul 156-756, Korea
(*Received 4 November 2011 • accepted 19 January 2012*)

Abstract–Macroporous silica (MS) and macro/mesoporous silica (MMS) were prepared by spray drying a polystyrene (PS) latex sol containing a silica source, followed by calcination. As a silica source, 3-aminopropyl triethoxysilane (APS) was used for MS while either silica sol (SS) or tetraethoxyothosilicate using P123 templating (P123-TEOS) was used for MMS. Spray drying and calcination could also take place in a once-through aerosol reactor. The transformation of the silicon alkoxides to silica and decomposition of PS occurred at similar temperatures. Therefore, for APS-originated MS, the metal additives such as silver and nickel were required to accelerate the former. In addition, the nickel was well dispersed in the silica matrix during calcination even at 800 °C, in turn to thermally stabilize the porous structures. The wall-preforming additives were unnecessary for PS/SS and PS/P123-TEOS, since the SS drying and P123 templating, respectively, took place at lower temperature than PS decomposition. The porosities of all the porous silica prepared ranged from 0.54 to 0.57, which were close to the volume fraction of PS in the PS-alkoxides mixture solidified right after spray drying.

Key words: Porous Media, Nanostructured Materials, Spray Drying, Spray Pyrolysis, Polystyrene Latex (PSL) Particles

INTRODUCTION

Macroporous materials have attracted much attention due to their potential applications in a wide range of fields on separation media, catalysts, photonic crystals, drugs and other nanodevices [1,2]. They have been fabricated by colloidal templating, which involves three common steps [1]. First, colloidal crystals are formed by self-assembling uniform spheres with the diameters greater than 50 nm into multi-dimensional arrays. Second, the interstitial space is infiltrated by a precursor to be converted to a solid wall. Finally, the spheres are removed by leaching or thermal decomposition, to leave macroscopic pores at the sites. Typical colloidal crystals were made of spheres of silica [3], polystyrene (PS) [4-12] and poly(methylmethacrylate) (PMMA) [13], respectively. The processes for colloidal crystallization [1] include gravitational settling [4-7,13], centrifugation [8], electrophoresis, mechanical pressing [3] and dip coating [10]. The porous structures prepared have been reported as face-centered cubic (fcc) or hexagonal close packing (hcp) occupying 74 volume% of the whole structure theoretically [1]. The actual porosity of the macrostructure was much lower because solvent evaporated before complete packing of the spheres and there existed some aggregation between them [8]. To produce macroporous silica (MS), the interstice between the colloidal crystals made of PS lattices was infiltrated by tetraethoxyothosilicate (TEOS) [4,6,8] and silica nanoparticles [5,13]. Mesoporous silica wall surrounding the macropores could be also prepared by surfactant templating to yield macro/mesoporous silica (MMS) [7]. However, those wet chemical preparations requiring numerous processing steps took several days to obtain the final MS. Recently, a facile aerosol route to the MS was developed in a two-stage furnace [10-12]. The suspension composed of PS spheres and silica nanoparticles was nebulized to enter a tubular reactor. In the first half of the reactor, as the aerosol droplets dried up by the solvent evaporation, the colloidal crystallization and subsequent infiltration of silica nanoparticles took place. In the second half, the colloidal crystals were removed by their decomposition. The entire process could be completed in only several seconds during the flight of the droplet in the reactor. Fan et al. [14] applied the rapid aerosol process for drying the precursor droplets followed by post calcination to prepare MMS using TEOS, Brij-56 and polystyrene latices. They discussed packing fractions of N monodisperse hard spheres by Monte Carlo simulations. While in the wet route the three steps, such as colloidal crystallization, silica infiltration and solidification, and colloidal crystal removal, took place consecutively with time margin. However, in the aerosol processing the entire processing should be finished in seconds. There would not be time enough for complete colloidal crystallization. In addition, the number of PS spheres in a droplet would not be enough for their self-assembly. There would be overlap between solid-wall formation and PS removal. Excessive heating might destroy the macroporous skeletons. To successfully prepare MS and MMS, the selection of silica precursor, control of the temperature history during the flight, and heat transfer rate between gas and droplets are essential. Even though there have been some successful results for preparations of MS and MMS by aerosol synthesis under the specific conditions, it has been not clear yet how to guarantee them in general conditions.

In the present study, aerosol synthesis has been applied with various silica sources such as 3-aminopropyl triethoxysilane (APS), silica sol and precursor for P123-mediated mesophase based on TEOS for wall materials under the same conditions. APS was challengingly chosen because its hydrolysis/condensation temperature is

†To whom correspondence should be addressed.
E-mail: sgkim@cau.ac.kr

similar to the PS decomposition temperature. Throughout the study we are focusing on obtaining the optimal conditions for the successful preparations of the MS and MMS with the highest porosities. We investigated how to form the well-organized macropores with high thermal stability and high porosity.

EXPERIMENTAL

1. Materials

All the materials used were reagent grade. Tetraethoxyorthosilicate (TEOS), hydrochloric acid, ethanol (95%) and nickel nitrate ($Ni(NO_3)_2 \cdot 6H_2O$, 98%) were purchased from Samchun Chemicals. 3-aminopropyl triethoxysilane (APS), sodium salt of dodecyl sulfate (SDB-Na), potassium peroxodisulfate ($K_2S_2O_8$), sodium triphosphate ($Na_5P_3O_{10}$), and styrene monomer were purchased from Sigma. Silver nitrate (99.9%) was purchased from Kojima Chemicals. Pluronic P123 ($PEO_{20}PPO_{70}PEO_{20}$) was gratefully gifted by BASF Korea. Silica sol was prepared by diluting colloidal silica (SS-SOL 30E) purchased from Shin Heung Silicate.

2. Preparation of Polystyrene Latex Spheres

A batch reactor with reflux was used to prepare monodisperse polystyrene spheres. In the reactor, 0.0975 g of SDB-Na, 0.325 g of $K_2S_2O_8$ and 32.5 mL of styrene monomer were dissolved in 186.5 mL D.I. water. Polymerization was carried out with magnetic stirring at 80 °C for 18 hours. The monodisperse PS spheres with the diameter of 80 nm were prepared in suspension. Sols with various PS concentrations were made by diluting the suspension as prepared (14.8 wt% PS) with deionized water.

3. Preparation of Precursor Suspensions

3-1. Macroporous Silica (MS) from PS/APS

The polystyrene sol as prepared was diluted with D.I. water to 0.5 wt% PS. 7.65 g APS and 1.7 g (0.01 mol) $AgNO_3$ (22.2% of APS in mass) were dissolved in 100 mL D.I. water. The silver nitrate was included to accelerate the solidification of APS, which will be described in the next section. The precursor sols for macroporous Ag-silica (MS/Ag-APS) were then prepared by mixing the diluted PS suspension and the $AgNO_3$-APS solution in a variety of the volume ratios around 18 : 1 (reference condition). Instead of silver, nickel was also added as nickel nitrate to APS for MS/Ni-APS. The same PS suspension was added to the mixed aqueous solution containing 6.54 g APS (reference condition) and 2.98 g (0.01 mol) $Ni(NO_3)_2 \cdot 6H_2O$ in the same manner. The mass of APS for each MS was determined in the previous study [15] as the minimum mass which can well disperse 0.01 mol of either silver or nickel particles in silica matrix.

3-2. Macro/Mesoporous Silica (MMS)

Two types of MMS were prepared: from PS-silica sol pair (PS/SS) [10-12]; and from the pair of PS and precursor for P123-templating mesoporous silica (PS/P123-TEOS). For the former (MMS/SS), 0.5 wt% PS sol was mixed with 0.1 wt% silica sol in different volume ratios around 1 : 1 (reference condition). For the latter (MMS/P123-TEOS), the sols with various concentrations of PS were prepared from the reference sol as-prepared (14.8 wt% PS). The precursor for the silica was composed of TEOS, HCl, EtOH and P123 with the molar ratio of 1 : 0.0004 : 22 : 0.012 [16]. 50 mL of the PS sol with predetermined PS concentration was then added to such solution having 7.31 mL TEOS and others in proportion.

4. Aerosol-phase Reaction

The porous silica was prepared by two methods. The first used the spray drying followed by calcination. In detail, the sols containing PS and silica source were ultrasonically sprayed by home humidifier (60 MHz and 35 W). The droplets were carried by nitrogen gas (99.9%) at 1 L/min into a tubular reactor (30 mm in diameter and 700 mm in length) heated at 150 °C. The particles were recovered by filtration at the outlet of the reactor. They were finally calcined in the nitrogen gas at 400 °C (reference condition) for 30 min, where either APS or TEOS completely transformed to silica, while polystyrene beads and P123 were all removed by decomposition. The calcination environment was changed to 10% H_2 and 90% N_2 at 600 °C (reference condition) in case of MS/Ni-APS. The second method to prepare MS utilized once-through aerosol reaction, where the entire process, including spray drying and calcination, was performed in a single tubular reactor. For this to happen, the tubular reactor was lengthened to 1,500 mm. It was heated in two segmented furnaces in series, each set at different temperatures. The first segment (900 mm) was kept at 100 °C, and the second segment (600 mm) was at either 600 °C or 800 °C. We investigated the effect of the process variables, such as the nature of metal precursor, the volume ratio of PS to silica precursor and calcination temperature, on the morphology of MS and MMS, especially the porosity of the final product spheres.

5. Characterization of Porous Silica

The porous structures were observed by transmission electron microscope (TEM, JEM-2000EX, JEOL) and scanning electron microscope (SEM, Philips Co, Philips 515), and analyzed by small angle X-ray spectroscopy (SAXS, GADDS, Brucker). The reduction state and crystallinity of silver and nickel nanoparticles in the matrix were investigated by X-ray diffractometer (XRD, SDS 2000, Scintag). Removal of PS and P123 was confirmed by thermogravimetric analyzer (TGA, MAC, Science, TG-DTA 200) and Fourier-transform infrared spectroscopy (FT-IR, Perkin Elmer FT-IR 1615). Specific surface area, pore volume and pore size distribution of the silica were measured by surface area and porosimetry analyzer (BET, ASAP 2010, Micrometrics).

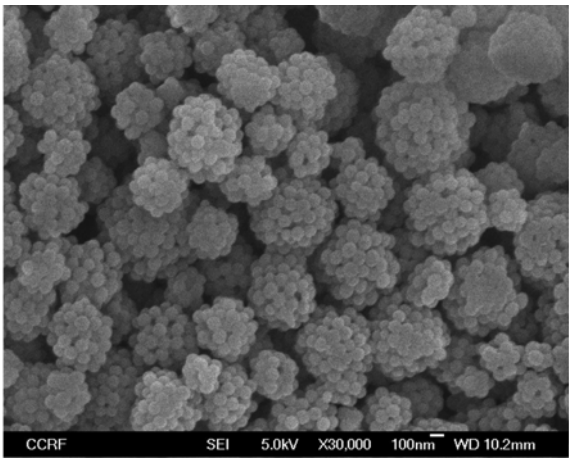

Fig. 1. SEM images of aggregates obtained from spray drying of 0.5 wt% PS sols at 150 °C, otherwise under reference conditions.

RESULTS

1. Drying/Calcination to Macroporous Silver-silica Composites

For comparisons later, 0.5 wt% PS sol was spray-dried without any silica source at 150 °C, whose image is shown in Fig. 1. In such pure PS agglomerates, the packing of the PS latex spheres looks random, supporting their good dispersion in the sol. This also showed that the hcp packing was hard to attain in this fast assembling process. The number average diameter of the aggregates was 600 nm. Then, 0.5 wt% PS sol and 7.65 wt% APS solution (PS/APS) without metal nitrate were mixed with the volume ratio of 18 : 1 and processed. The solid mass ratio of PS to APS was 9 : 7.65. The PS/APS particles obtained are shown in Fig. 2(a), where most macropores were collapsed. This reflected that the transformation from APS to silica took place no earlier than PS decomposition. To leave the pores having the same size of the PS latices, wall materials need to be rigid before PS are decomposed. The rest of Fig. 2 show the SEM images of MS/Ag-APS and MS/Ni-APS prepared under the reference conditions. The solid mass ratios of PS to APS+$AgNO_3$ and APS+$Ni(NO_3)_2$ were, all close to 1, 9 : 9.35 and 9 : 9.52, respectively. The addition of the metal nitrates clearly left robust macropores at the sites of polystyrene spheres. The clue to explain this is found in Fig. 3, which shows the thermogravimetric analyses of the four samples all just as spray-dried at 150 °C, otherwise under the reference conditions. The precursor used for each sample is indicated for the corresponding curve in the figure. The PS/SS curve shows that PS would decompose around 400 °C. The PS/APS curve shows a single and sudden decline around 400 °C revealing that PS decomposition and APS-to-silica transformation occur simultaneously. This explains why most macropores were collapsed as shown in Fig. 2(a). In the curves of PS/Ag-APS and PS/Ni-APS, the weight loss began sharply at 200 °C and continued up to ~500 °C. The sharp weight loss was related to the metal formation from its nitrate [17]. The following slow weight loss in a wide temperature range would mean that either APS transformation or PS decomposition took place at temperatures lower than 400 °C. Since the catalytic effect of metals on silica formation has been reported elsewhere [17], it is highly probable that APS transformed to silica at lower temperatures for PS/metal/APS. This supported that the robust pores were obtained by the inclusion of metals in silica matrix as shown in Fig. 2(b) and 2(c). Since metals have higher thermal conductivities than APS or PS, the high rate of heat transfer from hot gas to the metals would be also responsible for the lowering APS decomposition temperature. Fig. 4 shows the SEM images of MS/Ag-APS prepared from PS/$AgNO_3$-APS at various volume ratios of the PS sols to the mixed solution of $AgNO_3$ and APS, otherwise under the reference conditions. As shown in Fig. 2(b) and Fig. 4, most macropores were observed at PS sol-to-APS solution ratio of 18 : 1 (reference condition). At the ratio of 9 : 1 some pores were buried by silica. When the volume ratio increased to 36 : 1, corresponding to the solid mass ratio of PS : APS+$AgNO_3$=18 : 9.35, the porous agglomerates lose sphericity due to the insufficient amount of wall materials. Fig. 5 shows the TEM images of the MS/Ag-APS calcined at different temperatures. As shown in Fig. 5(a), the agglomerates as spray-dried look like those composed of PS latices only (Fig. 1). The evaporation of water would make the front of $AgNO_3$-APS pool retreat beneath the outmost layer of PS spheres. For the volume ratio of 18 : 1 $AgNO_3$ and APS would fill the interstice between PS latices up to a half of the outmost PS layer. By calcination at 400 °C and above, the PS spheres were all removed after APS completely transformed to silica.

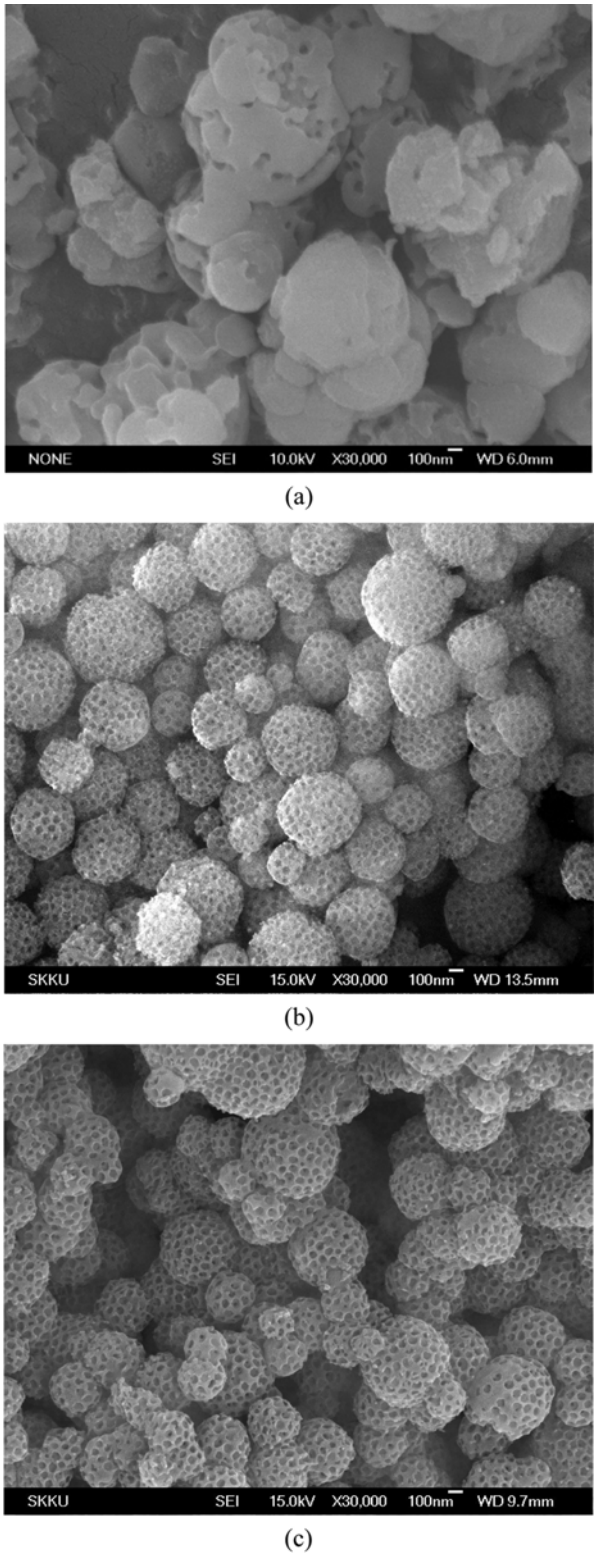

Fig. 2. SEM images of composites spray-dried at 150 °C and calcined at 600 °C for 30 min, otherwise under reference conditions. (a) No metal salt; (b) MS/APS-Ag; (c) MS/APS-Ni.

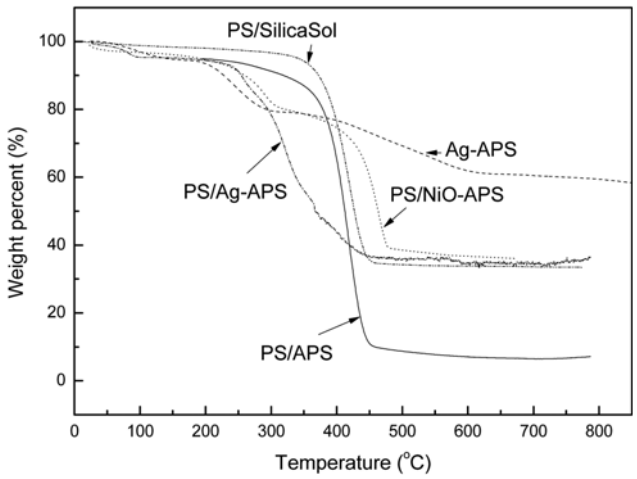

Fig. 3. Thermogravimetric analyses of the four samples as spray dried at 150 °C, otherwise under the reference conditions.

The FT-IR spectra, shown in Fig. 6, indicated that in the sample as spray-dried there was found some changes in APS peaks while PS-related peaks remained unchanged. At 400 °C PS peaks were all disappeared and there showed up the deep valley with shoulder around 1,100 cm^{-1}, the characteristic absorption peak of silica. This proved that the APS decomposition preceded PS removal. In Fig. 5, the dark spots, indicating silver nanoparticles, grew by sintering. Some overgrown silver particles escaped from the wall matrix at 800 °C, where the porous structures partially demolished [16]. The XRD pattern shown in Fig. 7 made sure that the crystalline silver excessively grew at 800 °C.

2. Drying/Calcination to Macroporous Nickel-silica Composites

As shown in Fig. 3, the PS/Ni-APS curve gave a sharp decrease in mass around 200°C due to the high reduction of molecular weight from the nitrate ($Ni(NO_3)_2 \cdot 6H_2O$, 290.8) to nickel (Ni, 58.7), compared to the silver counterpart (170 to 108). Due to the very low sintering characteristics of nickel, nickel crystalline peaks were very weak in MS/Ni-APS, even at 800 °C (not shown). The highest porosity was found at the ratio of 18 : 1 (reference condition) as shown in the Figure. The actual mass ratio of PS to APS+$Ni(NO_3)_2 \cdot 6H_2O$ was 9 : 9.52. The ratio of APS to $Ni(NO_3)_2 \cdot 6H_2O$ was 6.54 : 2.98 (0.01 mol), which was compared with 7.65 : 1.7 (0.01 mol) for APS to $AgNO_3$. The optimum mass of APS was determined with the mole of metal nitrate fixed. It was noted that the total masses of APS and nitrates turned out the same, and in turn the volumes were approximately the same, too. Fig. 8 shows the SEM and TEM images of MS/Ni-APS calcined at the different temperatures. The nickel nanoparticles, represented by dark spots in the TEM images, were well-dispersed in silica matrix, irrespective of the calcination temperature. They would not grow further up to 800 °C due to their low mobility compared to silver [17]. This would in turn contribute to retard the thermal deformation of the silica wall. The robust macropores of MS/Ni-APS were then observed even at 800 °C, as shown in Fig. 6(c).

Both the MS/Ag-APS and MS/Ni-APS macroporous composites had strong hystereses in their adsorption-desorption isotherms as shown in Fig. 9(a) to manifest their meso/macroporosity. The pore size distributions of the composites prepared with the optimum ratio of PS to APS and metal nitrates are shown in Fig. 9(b). The

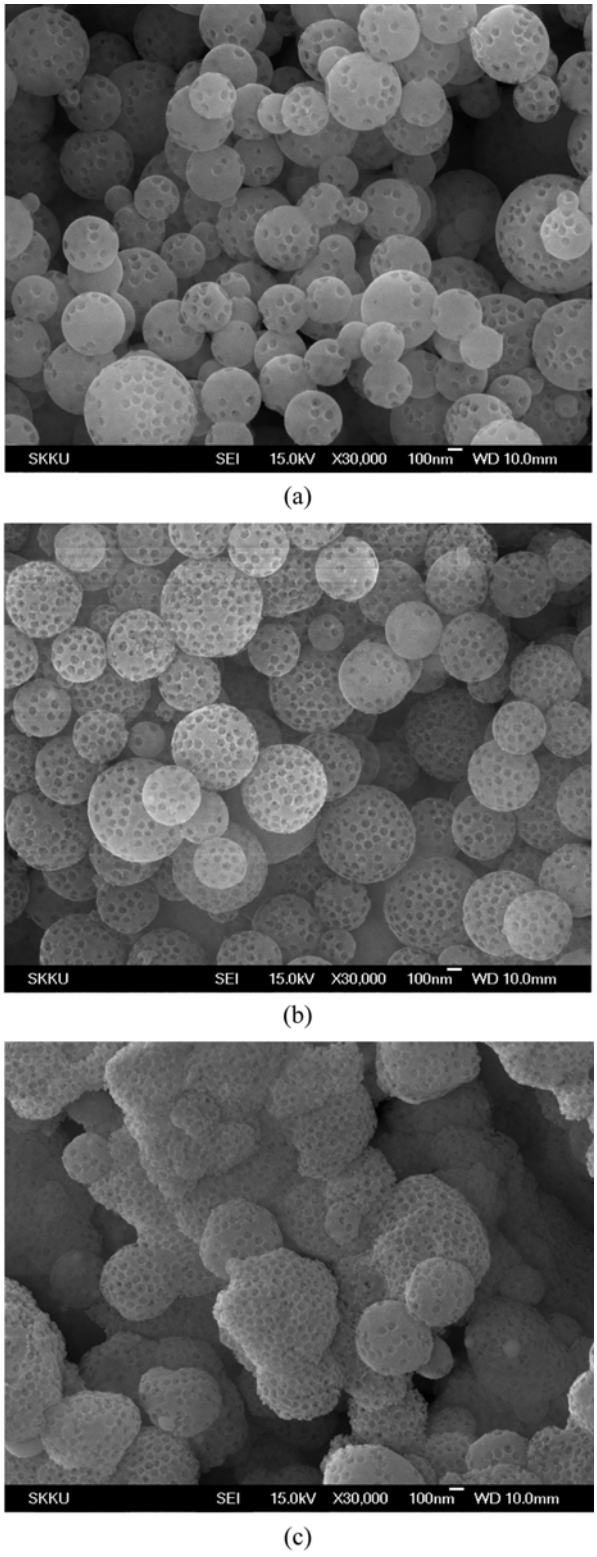

Fig. 4. SEM images of the MS/Ag-APS prepared at various volume ratios of 0.5 wt% PS sols to the mixed solution of 7.65 wt% APS and 1.7 wt% $AgNO_3$, otherwise under reference conditions. (a) 9 : 1; (b) 12 : 1; (c) 36 : 1.

modes in the pore size distributions are 80 and 50 nm for the silver-silica and nickel-silica, respectively. The pores in the MS-Ni-APS got smaller than those of the PS latices (80 nm) due to the silica sintering

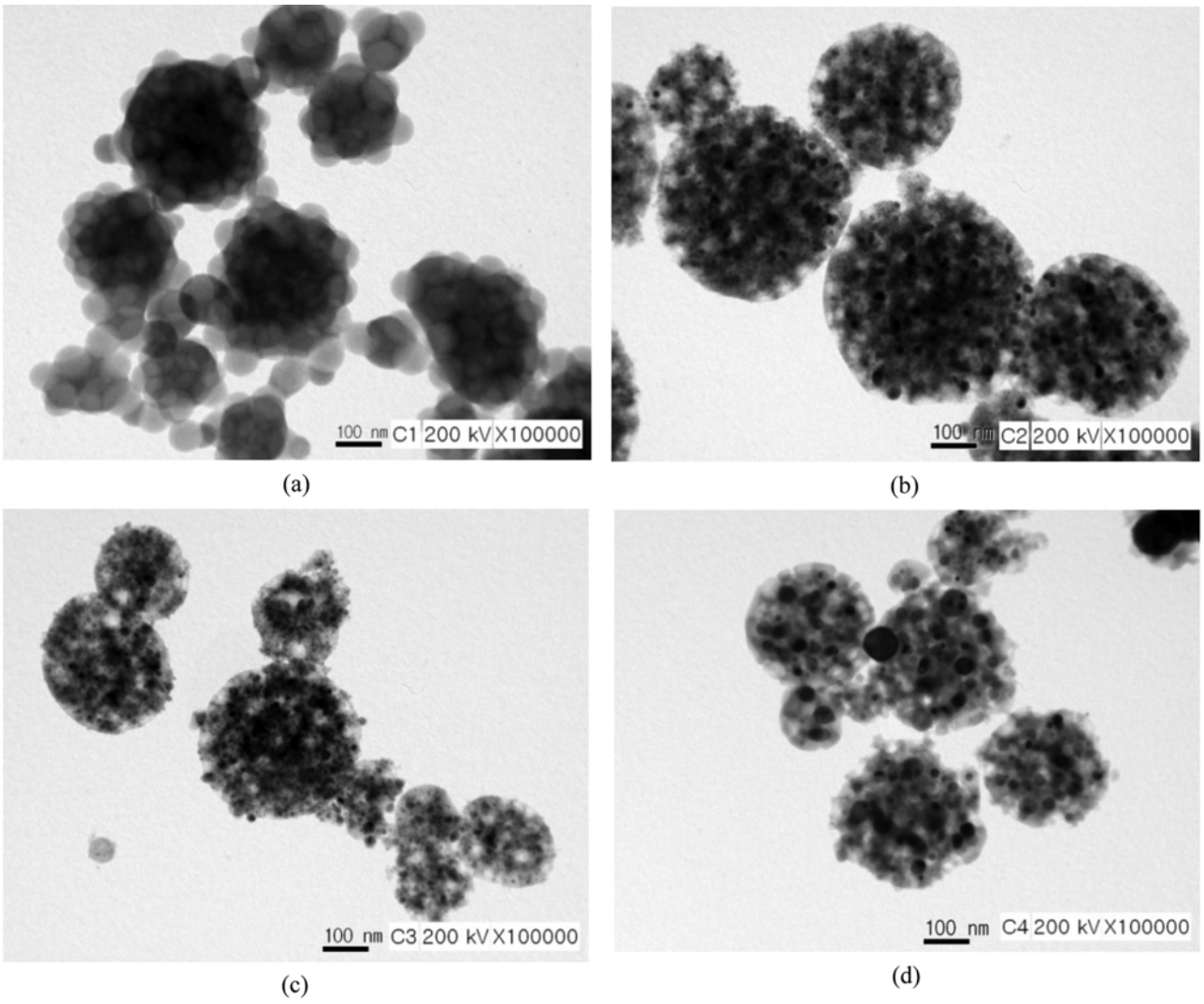

Fig. 5. TEM images of MS/Ag-APS calcined at different temperatures, otherwise under reference conditions. (a) As prepared; (b) 400 °C; (c) 600 °C; (d) 800 °C.

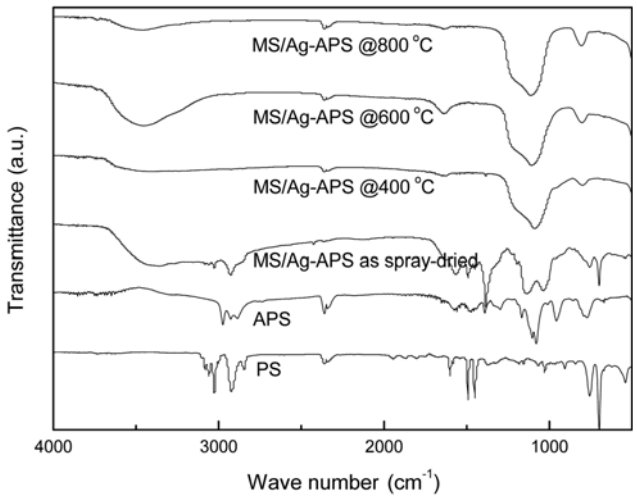

Fig. 6. FT-IR spectra of MS/APS-Ag calcined at different temperatures. Those of pure APS and PS are also shown in the same Figure.

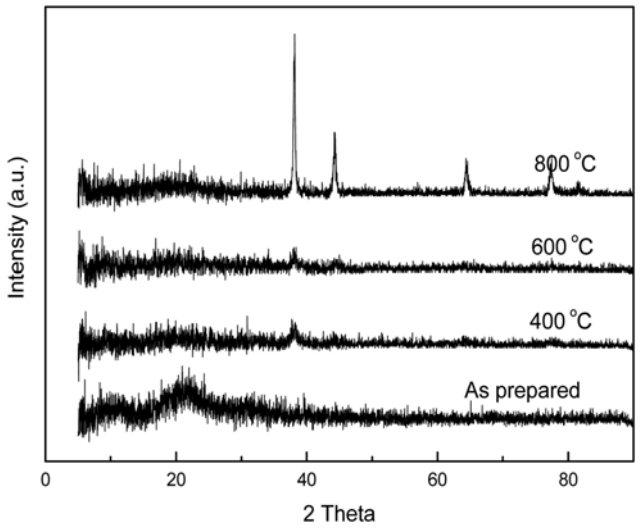

Fig. 7. XRD patterns of MS/Ag-APS calcined at different temperatures, otherwise under reference conditions.

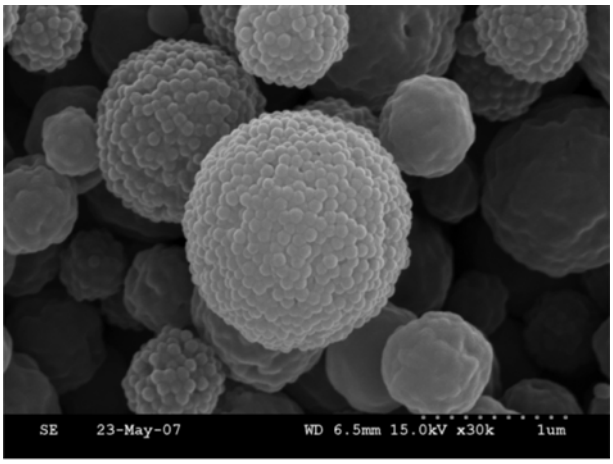

(a)

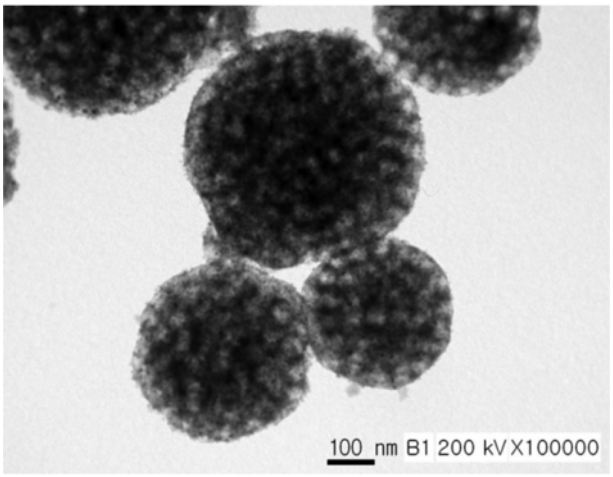

(b)

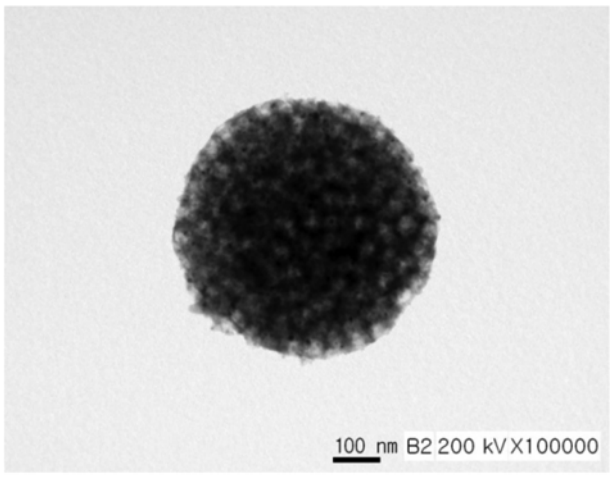

(c)

Fig. 8. SEM and TEM images of the MS/Ni-APS calcined at different temperatures, otherwise under reference conditions. (a) As prepared; (b) 600 °C; (c) 800 °C.

during the calcination. In contrast, as the silver came out of the silica matrix by calcination, the sintering of the silica preferentially filled the sites left by silver in the silica matrix. This left the pore size of MS-Ag-APS approximately at the size of PS sphere. Table 1 shows BET

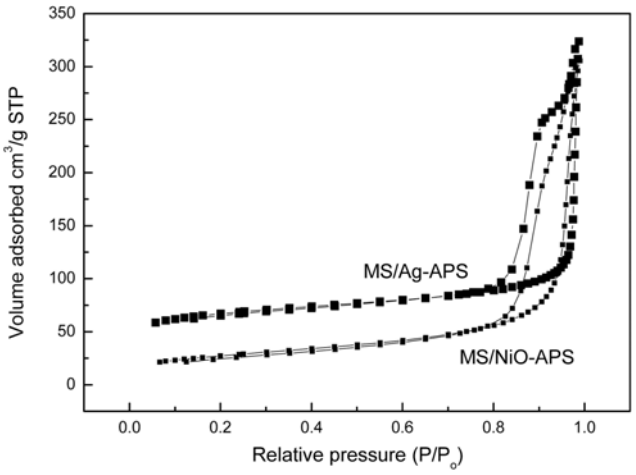

(a)

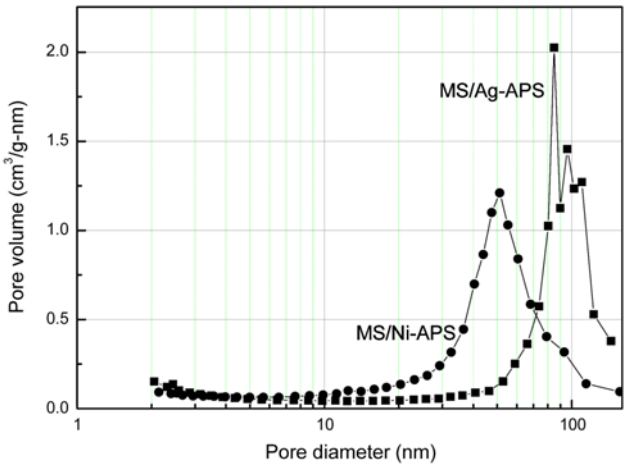

(b)

Fig. 9. (a) Adsorption-desorption isotherms and (b) pore size distributions for MS/Ag-APS and MS/Ni-APS prepared under reference conditions, respectively.

results of some MS and MMS. For MS/Ag-APS, there existed large differences between single-point method and BJH methods in surface area and average pore diameter. This suggested that the macroporous silver-silica has many small to medium mesopores compared to the macroporous nickel silica. Besides those pores, the values related to pores are very similar in two macroporous materials.

3. Once-through Process to Macroporous Metal-silica Composites

Robust macroporous silica spheres were also obtained in the 1,500-mm aerosol reactor heated by the two-segmented furnace, the first 900-mm segment set at 100 °C and the second 600-mm segment set not less than 600 °C, as described before. The temperature for PS decomposition increased from 400 °C to 600 °C, due to the short residence time compared to batch calcination. The TEM images of the two composites prepared at 100-600 °C are shown in Fig. 10. In the first 100 °C-zone the droplets were completely dried while the metal nitrate was solidified in the interstice between the assembled PS lattices. In the second 600 °C-zone (600 mm long), the metal was formed in APS pool, then APS completely solidified to silica and in turn the PS latex spheres decomposed, leaving the macropores

Table 1. BET data for MS and MMS prepared under reference conditions

	Porous structure	MS/Ag-APS	MS/Ni-APS	MMS/SS	MMS/P123-TEOS
Area m^2/g	BET surface area	232.0980	98.7229	151.3977	347.8005
	BJH adsorption cumulative surface area of pores (1.7-300 nm)	85.6893	91.0012	149.2580	255.0070
	BJH adsorption cumulative surface area of pores (1.7-300 nm)	110.1368	103.6201	169.4995	476.3366
Volume cm^3/g	Single Point adsorption total pore volume of pores less than 175.3 nm	0.475277	0.457702	0.222915	0.581628
	BJH adsorption cumulative pore volumes of pores (1.7-300 nm)	0.437388	0.477284	0.218108	0.536456
	BJH adsorption cumulative pore volumes of pores (1.7-300 nm)	0.454347	0.473887	0.230763	0.594180
Pore size nm	Adsorption average pore diameter	8.19097	18.54490	5.88952	6.68921
	BJH adsorption average pore diameter	20.41739	20.97924	5.84510	8.41480
	BJH desorption average pore diameter	16.50117	18.29327	5.44570	4.98960

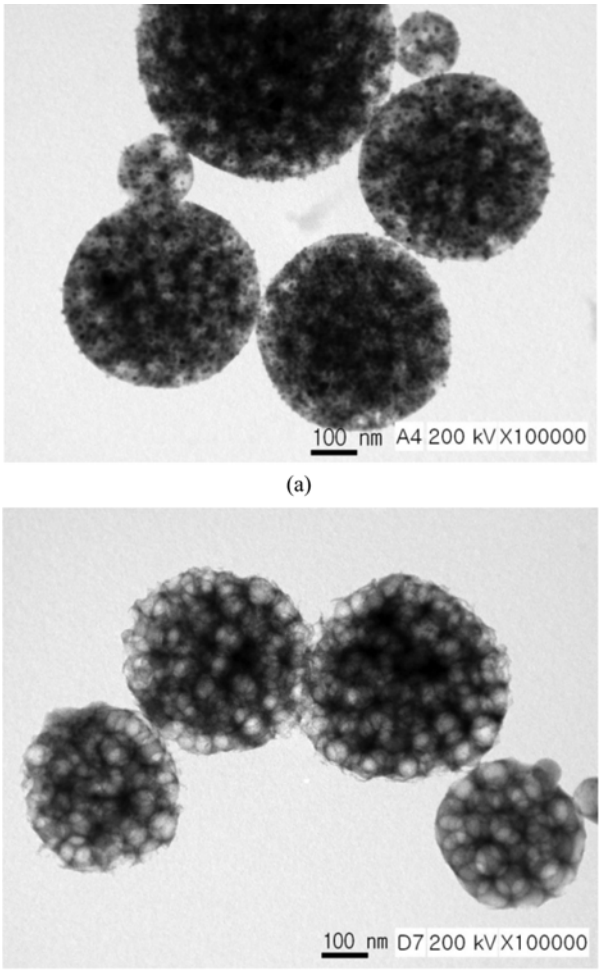

Fig. 10. TEM images of (a) MS/Ag-APS and (b) MS/Ni-APS prepared in once-through aerosol reactor having two-stage heating zone maintained at 100-600 °C, otherwise under reference conditions.

at their sites.

4. Macro/Mesoporous Silica (MMS)

MMS/SS was prepared by varying the volume ratio of the 0.5 wt% PS sol to 0.1 wt% silica sol, similarly to the method of Iskandar et al. [11]. Some macro/mesoporous spheres were, however, broken severely in our experiment due to the aggregation of silica nanoparticles and in turn low mechanical strength. The robust macropores were obtained at the volume ratio of 1 : 1. The specific surface area, pore volume and average pore diameter are 151 m^2/g, 0.22 cm^3/g and 5.89 nm as shown in Table 1. The existence of mesopores was proved by the fact that the specific surface area was higher and the pore size was lower than those of either MS/Ag-APS or MS/Ni-APS. However, the excessive reduction in the pore volume was caused by the severe breakup of the macro/mesoporous structures.

Fig. 11 gives the TEM images of the MMS/P123-TEOS prepared from the mixture of PS sol and precursor solution for P123-templating mesophase (PS/P123-TEOS) by varying the weight % of PS in the sol. The preparation was similar to the method of Fan et al. [14]. As shown in the figure, the macropores were well surrounded by the wall of the mesoporous silica. This indicated that any wall-forming additive such as metal was not necessary, since the early P123-templating was enough to maintain the rigid wall. When 10 wt% PS sol was used, the external surface of the spheres was covered with the mesoporous silica so that the macropores might be hidden beneath the surface. For 12 wt% PS sol the outmost macropores would be just tangent to the external silica surface. A well-dimpled macro/mesoporous structure was obtained for 14.8 wt% PS sol (reference condition). This meant that the level of silica pool went down by a radius of outer PS latex spheres, which disappeared during calcination, as described before. When the % of PS reached 20, silica concentration was too low to fill the interstice. Then some macrostructures were broken.

The specific surface area of the MMS/P123-TEOS obtained with 14 wt% PS sol was as high as 348 m^2/g, the highest of the four spheres shown in Table 1, representing the existence of mesopores in addition to the macropores. Some differences in surface area were found between the methods of calculation, again supporting the existence of small or medium mesopores. Probably due to this, the pore volume of MMS/P123-TEOS was higher and the pore diameter was smaller, than those of MS/metal-APS. Fig. 12 shows the adsorption-desorption isotherms and pore size distributions for MMS/P123-TEOS and mesoporous silica [10], all prepared otherwise under the reference conditions. As illustrated in the Fig. 12(a), the area of the hysteresis loop for the former was smaller than that of the latter, indicating the relative reduction of the mesopores at least by number. Fig. 12(b) shows that the pore size distribution of MMS/P123-TEOS was clearly bimodal at 6.5 nm and 49 nm. The diameter of the mesopores was

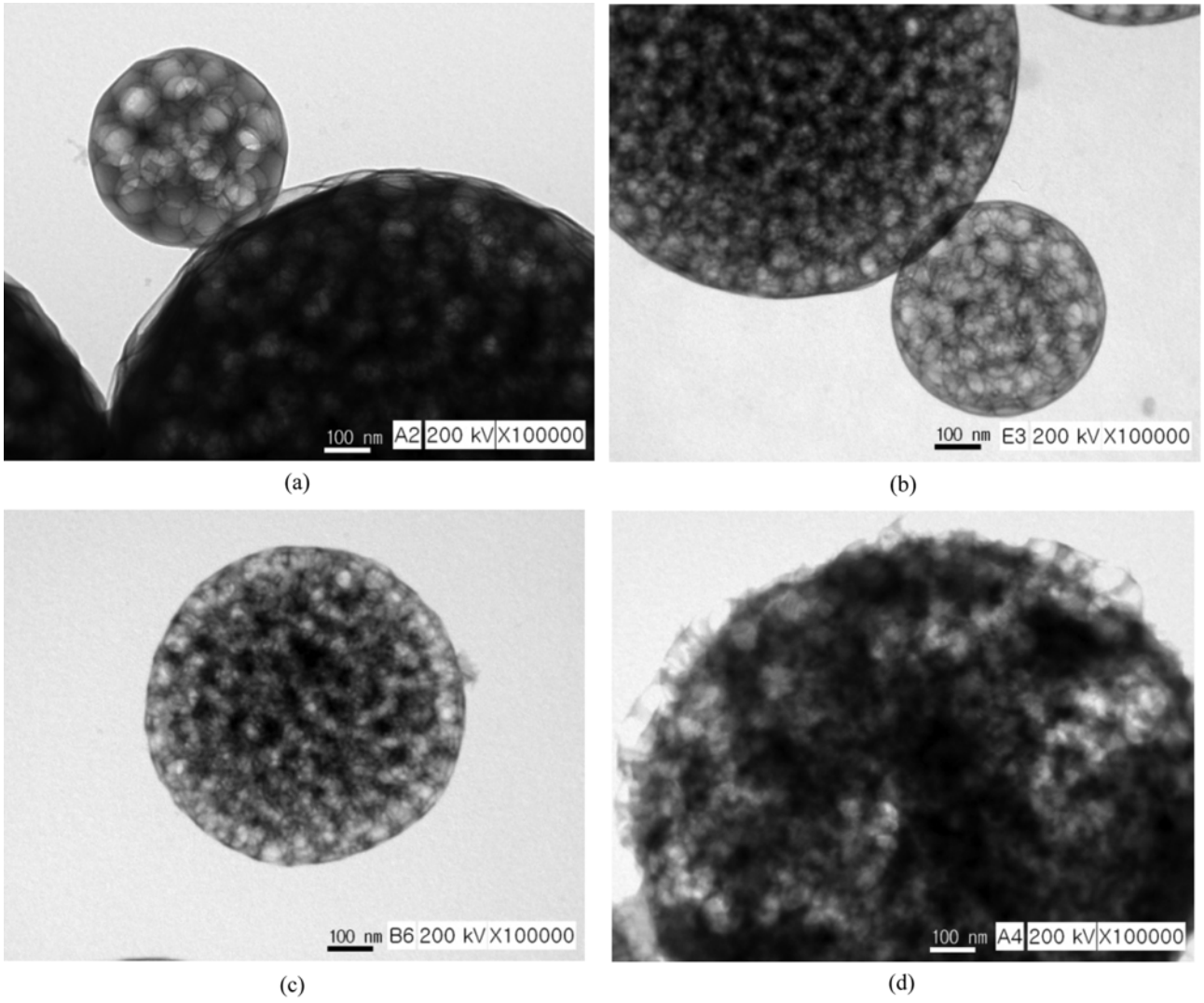

Fig. 11. TEM images of MMS/P123-TEOS prepared from the mixture of PS sol and precursor solution for P123-templating mesophase by varying the weight % of PS in the sol, otherwise under reference conditions. (a) 10 wt%; (b) 12 wt%; (c) 14.8 wt%; (d) 20 wt%.

considerably reduced from 11.6 nm for pure mesoporous silica to 6.5 nm as the mesopores were formed in the interstice between mesostructures. This was probably explained by the nanosize effect of the mesophase wall thickness.

5. Volume Ratio of PS to Wall Materials

From the pore volume data (cm^3/g solid) in Table 1 the porosities of three porous structures prepared under the reference conditions were calculated. The data of the MMS/SS were excluded, due to the considerable breakup of the structures. There was assumed the additivity of the constituent volumes and the bulk densities of the constituents were used. The porosities calculated for MS-Ag-APS and MS-Ni-APS were 0.589 and 0.554, respectively. The macro/mesoporosity of MMS/P123-TEOS was given as 0.592. These values coincided with the value (0.56) calculated by MC simulation [14]. They were all lower than the solidity of random aggregates of monodisperse spheres (~0.6) and much lower than the hcp (or fcc) packing fraction of 0.74. Such low values were explained by the incomplete packing, aggregation of PS latices, and finite size ratio of PS latex to the macroporous sphere as well as the high surface curvature of the sphere. The porosities were then calculated from the solid volume ratio of PS latices to the wall materials. The volume of the wall materials could vary from that of the precursor materials (metal nitrates, APS, P123 and TEOS) to that of the products (nickel, silica). The porosities calculated based on the latter were 0.678, 0.716 and 0.78 for MS/Ag-APS, MS/Ni-APS, MMS/P123-TEOS, respectively, considering the volume contraction of PS latices (80 nm to 50 nm), as described above. On the other hand, the porosities calculated based on the former were 0.54, 0.52 and 0.56 for MS/Ag-APS, MS/Ni-APS, MMS/P123-TEOS, respectively. These were quite close to those calculated from BET data. This suggested that the final porosities were determined during the initial drying stage. In other words, the volume ratio of PS to solid precursor in the dried composite spheres did not change even though the transformation took place.

CONCLUSION

Various types of MS and MMS were prepared based on the aero-

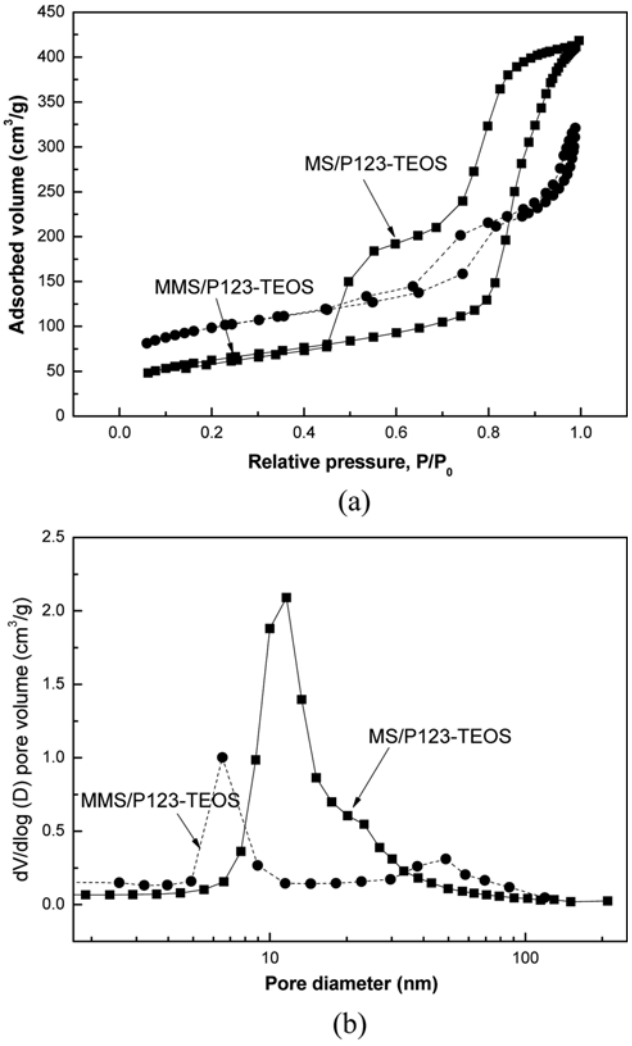

Fig. 12. (a) Adsorption-desorption isotherms and (b) pore size distributions for mesoporous silica and MMS/P123-TEOS, otherwise under reference conditions.

sol-phase drying followed by calcination. To leave the macropores at the sites of the self assembled PS when APS was used for infiltrating materials, the addition of silver and nickel nitrates was required. The metals, once formed around 200 °C, accelerated the transformation of APS to silica, before PS decomposed at 400 °C. This enabled the use of once-through reactors to produce the robust macroporous spheres. The silver easily escaped from silica wall by high-temperature calcination. On the other hand, low mobile nickel was well dispersed in silica matrix up to 800 °C. This made the thermal stability of MS/Ni-APS higher than that of MS/Ag-APS. The mixture of PS and silica sols was simply spray-dried to give MMS/SS by removing PS. However, the wall structure was apt to be broken due to its mechanical weakness. Macro/mesoporous spheres could be prepared where macropores were surrounded by P123-mediated mesoporous silica. Here, the P123 played the dual roles as a templating agent and wall-forming aid. The porosities were 0.55 to 0.59, close to the volume ratio of PS to the solid precursors right after spray drying, approaching to the solidity of randomly packed spheres (0.6).

ACKNOWLEDGEMENT

This work was supported by the Chung-Ang University Research Scholarship Grants in 2010.

REFERENCES

1. A. Stein, *Micropor. Mesopor. Mater.*, **44-45**, 227 (2001).
2. A. Stein and R. C. Schroden, *Curr. Opin. Solid St. M.*, **5**, 553 (2001).
3. S. A. Johnson, P. J. Olliver and T. E. Mallouk, *Science*, **283**, 963 (1999).
4. Q.-Z. Wu, Q. Yin, J. F. Liao, J.-H. Deng and Y.-G. Li, *Chinese J. Chem.*, **23**, 689 (2005).
5. Y.-W. Chung, I.-C. Leu, J.-H. Lee and M.-H. Hon, *J. Alloy Compd.*, **433**, 345 (2007).
6. Q.-Z. Wu, J. Liao, Q. Yin and Y.-G. Li, *Mater. Res. Bull.*, **43**, 1209 (2008).
7. B. Lebeau, C. E. Fowler, S. Mann, C. Farcet, B. Charleux and C. Sanchez, *J. Mater. Chem.*, **10**, 2105 (2000).
8. D. A. B. Filho, C. Hisano, R. Berthodo, M. G. Schiavetto, C. Santilli, S. J. L. Ribeiro and Y. Messaddeq, *J. Colloid Interface Sci.*, **291**, 448 (2005).
9. G-R. Yi, J. H. Moon and S. B. Yang, *Chem. Mater.*, **13**, 2613 (2001).
10. A. B. D. Nandiyanto, N. Hagura, F. Iskandar and K. Okuyama, *Acta Mater.*, **58**, 282 (2010).
11. F. Iskandar, M. Abdullah and K. Okuyama, *Nano Lett.*, **1**, 231 (2001).
12. L. Gradon, S. Janeczko, M. Abdullah, F. Iskandar and K. Okuyama, *AIChE J.*, **50**, 2583 (2004).
13. J. Liu, Y. Cai, Y. Deng, Z. Sun, D. Gu, B. Tu and D. Zhao, *Micropor. Mesopor. Mater.*, **130**, 26 (2010).
14. H. Fan, F. V. Swol, Y. Lu and J. Brinker, *J. Non-crystal. Solids*, **285**, 71 (2001).
15. K. H. Lee, PhD Dissertation, Chung Ang Univ. (2006).
16. S. H. Ye and S.-G. Kim, *Korean J. Chem. Eng.*, **27**, 1316 (2010).
17. K. W. Ahn, J. Y. Hyun and S.-G. Kim, *Aerosol Sci. Technol.*, **46**, 419 (2012).